AGU PUBLICATIONS

Geophysical Research Letters

RESEARCH LETTER
10.1002/2014GL060785

Key Points:
- Model results closely agree with MGS observations
- Ion escape rates slowly vary with rotation
- Crustal field has strong influence on the ionospheric structures

Correspondence to:
Y. Ma,
yingjuan@igpp.ucla.edu

Citation:
Ma, Y., X. Fang, C. T. Russell, A. F. Nagy, G. Toth, J. G. Luhmann, D. A. Brain, and C. Dong (2014), Effects of crustal field rotation on the solar wind plasma interaction with Mars, *Geophys. Res. Lett.*, *41*, 6563–6569, doi:10.1002/2014GL060785.

Received 4 JUN 2014
Accepted 21 AUG 2014
Accepted article online 24 AUG 2014
Published online 1 OCT 2014

Effects of crustal field rotation on the solar wind plasma interaction with Mars

Yingjuan Ma[1], Xiaohua Fang[2], Christopher T. Russell[1], Andrew F. Nagy[3], Gabor Toth[3], Janet G. Luhmann[4], Dave A. Brain[2], and Chuanfei Dong[3]

[1]Institute of Geophysics and Planetary Physics, University of California, Los Angeles, Los Angeles, California, USA, [2]Laboratory for Atmospheric and Space Physics, University of Colorado, Boulder, Colorado, USA, [3]Space Physics Research Laboratory, University of Michigan, Ann Arbor, Michigan, USA, [4]Space Science Laboratory, University of California, Berkeley, Berkeley, California, USA

Abstract The crustal remnant field on Mars rotates with the planet at a period of 24 h 37 min, constantly varying the magnetic field configuration interacting with the solar wind. Until now, there has been no self-consistent modeling investigation on how this varying magnetic field affects the solar wind plasma interaction. Here we include the rotation of this localized crustal field in a multispecies single-fluid MHD model of Mars and simulate an entire day of solar wind interaction under normal solar wind conditions. The MHD model results are compared with Mars Global Surveyor (MGS) magnetic field observations and show very close agreement, especially for the field strength along almost all of the 12 orbits on the day simulated. Model results also show that the ion escape rates slowly vary with rotation, generally anticorrelating with the strength of subsolar magnetic crustal sources, with some time delay. In addition, it is found that in the intense crustal field regions, the densities of heavy ion components enhance significantly along the MGS orbit, implying strong influence of the crustal field on the ionospheric structures.

1. Introduction

Mars has a spatially varying crustal field [*Acuna et al.*, 1998]. The intense crustal sources as detected by the Mars Global Surveyor (MGS) are mainly concentrated in the southern hemisphere in the Terra Sirenum region in the longitude range of 150°E to 240°E and latitude range of 30°S to 85°S [*Acuna et al.*, 1999; *Connerney et al.*, 1999]. As Mars rotates, different magnetic stresses contribute to the dayside ionospheric thermal pressure to counterbalance forces exerted by the solar wind plasma [*Brain*, 2006]. This could modulate the plasma environment around Mars and also has a potential to alter the ionospheric plasma escape rate.

Using Mars Global Surveyor (MGS) premapping data, *Crider et al.* [2003] found that the magnetic pileup boundary (MPB) is located higher in the southern hemisphere than in the northern hemisphere, suggesting that crustal magnetic fields have strong influence on the plasma boundary. This was confirmed later by *Brain et al.* [2005], who used more than 5 years of MGS data and showed that during southern summer, strong crustal fields near the subsolar point raise the altitude of the MPB over the entire dayside, implying that Martian crustal fields modify the solar wind interaction globally.

Observational data have also been used to investigate relations between plasma escape rates and the crustal field. Using data from Analyzer of Space Plasmas and Energetic Atoms 3 on Mars Express, *Lundin et al.* [2011] examined ion flux intensity patterns when the strong crustal magnetic field is located at different local times, and they found high fluxes of energized ionospheric O^+ on the dayside when the strong crustal field is near noontime. However, they found no discernible hemispheric difference in the total escape flux through the tail. *Nilsson et al.* [2011] used more than 4 years of Mars Express ion data to examine heavy ion escape from different positions in near-Mars space and found that the escape rate is statistically significantly higher from the northern quadrant than from the southern quadrant, indicating that the strong crustal field anomalies in the southern hemisphere cause the reduced ion outflow. Both studies suggest that the crustal field has a strong influence on the ion flow patterns; however, it is still unknown how the total plasma escape varies as the planet rotates or whether different ions have similar responses due to limited data coverage. This has been partly examined using numerical models in the past with steady state approximations [*Ma and Nagy*, 2007; *Fang et al.*, 2010], in which a limited number of cases were simulated for the same solar wind condition but with different subsolar longitudes. It was found that escape fluxes are the weakest when the strongest crustal source is facing the Sun. Although these earlier numerical studies provide some basic ideas about how the crustal fields affect

ionospheric escape, in reality, the subsolar longitude continuously varies with time; thus, the system may never achieve a steady state. In other words, the steady state approximation may not be able to fully represent the real situation. Even though the bow shock and the MPB adjust almost instantaneously to the new solar wind conditions as suggested by *Modolo et al.* [2012], a recent study of *Ma et al.* [2014] showed that ionospheric escape rates depend not only on current solar wind dynamic pressure but also on the earlier solar wind conditions and that it could take a few hours for the ionospheric/atmospheric system to reach a new quasi-equilibrium state.

Numerous global models have been applied to Mars [see reviews of *Nagy et al.*, 2004; *Ledvina et al.*, 2008; *Brain et al.*, 2010; *Kallio et al.*, 2011, and references therein]; those earlier numerical studies are usually restricted to stationary situations under various steady conditions of the solar wind and solar radiation. Until now, there has been no self-consistent modeling investigation on how this varying magnetic field affects the solar wind plasma interaction. To do that, the crustal fields and their rotation have to be included in the model. The inclusion of the crustal field rotation is time-consuming, because the model has to be run in time-accurate mode for at least a Martian day as opposed to obtaining a steady state solution with efficient algorithms (local time stepping). In this paper, for the first time, we will show how the rotation affects the solar wind plasma interaction process and how accurate the steady state approximation is when evaluating the ion escape rates. The model used in the study is briefly discussed in section 2. Model results and comparisons with MGS observations are presented in section 3. A short summary is presented in section 4.

2. Model Description

A multispecies single-fluid MHD model of Mars is used for the time-dependent calculation employing the University of Michigan Block-Adaptive Tree Solar Wind Roe Upwind Scheme (BATS-R-US) code [*Powell et al.*, 1999; *Toth et al.*, 2012]. The MHD model has been described in detail by *Ma et al.* [2004]. The model calculations are performed in the Mars-centered Solar Orbital (MSO) coordinate system: the x axis points from Mars to the Sun, the y axis points antiparallel to Mars' orbital velocity, and the z axis completes the right-handed coordinate system. In order to compare with MGS observations, the rotation axis of Mars is chosen to be that for a specific day on 16 May 2005. On this day, the rotation axis is tilted in both negative x and negative y directions in the MSO coordinates. The rotation axis vector is taken to be (−0.23, −0.36, and 0.90) in the coordinates, corresponding to the value in the middle of the selected day. The tiny variation of the rotation axis over the course of the day is neglected. At the beginning of the day on 16 May 2005, the subsolar location is 58.9°W, 13.0°S; the season on Mars during that time was between southern spring and southern summer. The rotation period relative to the Sun was 24.664 h, slightly longer than the sidereal day.

The computational domain is set to be $-24\ R_M < x < 8\ R_M$, $-16\ R_M < y$, and $z < 16\ R_M$, where R_M is the radius of Mars (3396 km). We use a nonuniform, spherical grid structure with the radial resolution varying from 10 km at the inner boundary (100 km altitude) to ~630 km near the outer boundary. The angular resolution is 3° in both longitudinal and latitudinal directions throughout the computation domain. The total number of cells is slightly over 1.1 million. This grid has a similar radial resolution in the ionosphere but coarser angular resolution than the one used in the work of *Ma et al.* [2004], so that the time-dependent calculation can be performed with reasonable computational resources. The inner boundary conditions are the same as used in *Ma et al.* [2004]. The time step is $dt = 0.02$ s. The crustal field is calculated based on the 60-order spherical harmonics from *Arkani-Hamed* [2001] and is updated every 4 min corresponding to ~1° rotation, which is smaller than the 3° angular resolution used in the calculation. Typically, the simulation requires 30,000 CPU hours to finish one Mars rotation. In order to avoid the possible influence from the initial condition, we use the preconditioning technique by starting the simulation 4 h before the time of interest.

No solar wind monitor is available for Mars, so we simply assume that the solar wind has typical values $n_{SW} = 4\ \mathrm{cm}^{-3}$, $U_{SW} = 400$ km/s, $T_P = 3.5 \times 10^5$ K, $B_X = 1.6$ nT, and $B_Y = -2.5$ nT (corresponding to the 3 nT Parker spiral magnetic field) and does not vary with time. This set of parameters corresponds to a dynamic pressure of 1.1 nPa and magnetosonic Mach number of 5.7. Based on the small sunspot numbers for year 2005, the photoionization rates used in the calculation correspond to solar minimum conditions [*Ma et al.*, 2004].

3. Model Results

We first compared the magnetic field from the model (blue lines) with MGS in situ observations (black lines) along the spacecraft trajectory, as shown in Figure 1. The model results (especially the magnetic field strength) closely

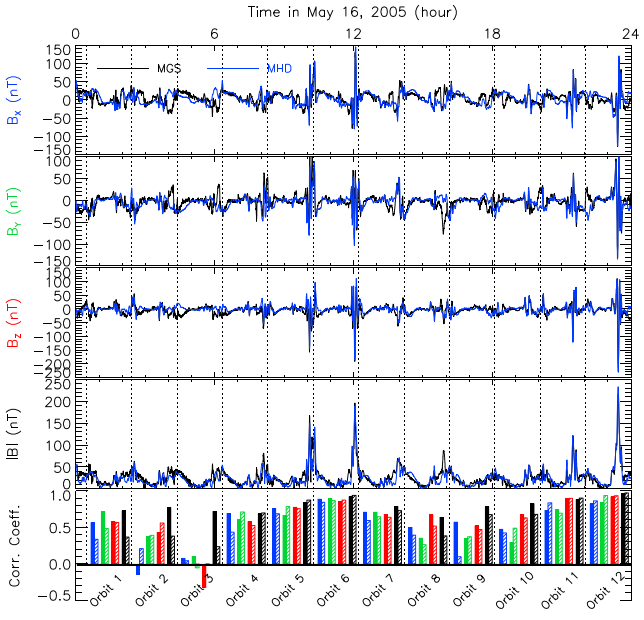

Figure 1. Comparison with MGS magnetometer observations along the spacecraft orbit during 16 May 2005. The black line shows the MGS observations, while the blue line is from the time-dependent multispecies single-fluid MHD model with rotation of the crustal field included. The color bars in Figure 1 (bottom) are the correlation coefficients for B_X (solid blue), B_{0X} (blue lines), B_Y (solid green), B_{0Y} (green lines), B_Z (solid red), B_{0Z} (red lines), B (solid black), and B_0 (black lines), respectively, for each corresponding orbit as separated by the vertical dashed lines.

follows the corresponding MGS observations. To quantify the comparison, we calculated the correlation coefficient, the root-mean-square error (RMSE), and the normalized root-mean-square error (nRMSE) for magnetic field components and strength for the whole time period using 10 s average data. The nRMSE is calculated using RMSE divided by the root-mean-square of the variable. The results are listed in Table 1. As shown in the table, the agreement is the best for B magnitude (corresponding coefficient = 0.88, RMSE = 10.8 nT, and nRMSE = 0.32). The excellent agreement between model and data for B magnitude suggests that during the entire day, the solar wind pressure was fairly steady and was similar to the input dynamic pressure used in the model. The agreement for the magnetic field components is also very good considering the fact that the solar wind magnetic field orientation is unknown and could be variable.

We make similar calculations for each of the 12 MGS orbits during the day, and the corresponding correlation coefficients for both the calculated magnetic field from the MHD model and the crustal field model are plotted at the bottom of Figure 1. We also plotted the geographic longitude-latitude map of the Martian crustal field with the MGS orbits superposed as supporting information to provide additional information for the geometry of MGS orbits. The start of each orbit is defined by the northward crossing of the MSO equator on the dayside as indicated by the vertical dashed lines. The correlation coefficients, in general, are fairly high ($>$0.60 for most cases); however, they do vary significantly from orbit to orbit, especially for the field components. The best correlation coefficient exceeds 0.9 for all the field components and reaches 0.98 for the field strength for orbit 12. This indicates that solar wind interplanetary magnetic field (IMF) is roughly in the same direction as the Parker spiral that is used in the calculation during the orbit. For orbit 2 and orbit 3, the simulated B_x and B_z components anticorrelate with the observations with negative coefficient, respectively. It is likely that during those two orbits, the actual solar wind IMF was in the opposite direction than the one used in the calculation, or it was highly variable during the orbit period. The range of the correlation coefficient for the magnetic field strength ranges from 0.65 to 0.98, showing very good agreement for all of the 12 orbits of the day. We also calculated the P values to determine the statistical significance of the correlation coefficients, and we found that they are all statistically highly significant (with $p < 0.001$, meaning that there is less than one in a thousand chances of not being correlated) except for the B_x component in orbit 3, which gives a P value of 0.015 (still indicating that it is statistically significant). As for all orbits, the P value is sufficiently low to ensure significant statistics; we conclude that the MHD model results are in close agreement with the observations. Also for most of the orbits, the calculated magnetic field (including both vector components and field strength) from the MHD model has significantly

Table 1. Correlation Coefficient, Root-Mean-Square Errors (RMSE), and Normalized RMSE for Magnetic Components and Strength for the Whole Time Period Using 10 s Average Data

	Correlation Coefficient	RMSE (nT)	nRMSE
B_x	0.64	16.1	0.82
B_y	0.65	14.4	0.80
B_z	0.76	14.3	0.68
B	0.88	10.8	0.32

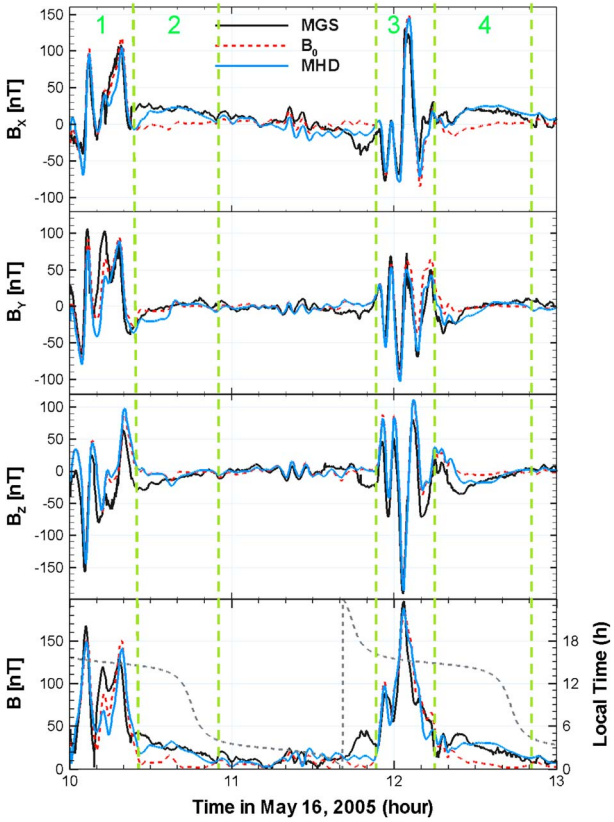

Figure 2. Zoom-in view of the comparison between model and observations for a 3 h period. The black line shows the MGS observations, the red dashed line is the crustal magnetic field B_0, and the blue line is from the MHD model. The gray dashed line in Figure 2 (bottom) is the corresponding local time for the MGS spacecraft. The green dashed lines separate strong (1 and 3) and weak (2 and 4) crustal field regions along the MGS trajectory.

higher correlation coefficients with the MGS observations as compared with the pure crustal field. We also note that for some orbits (such as orbits 5, 6, 11, and 12), the correlation coefficients of the pure crustal field are as good as those calculated using the MHD magnetic field results. This happens when MGS passed strong crustal field regions (with $B_0 > 100$ nT), so the induced fields are only a small contribution to the total fields. As a result, even though we see the improvement of the agreement during certain periods when the crustal field is weak (see Figure 2 for example), the overall correlation coefficients for those orbits are not noticeably improved by considering the induced fields from the model.

Figure 2 shows a 3 h zoom-in view of the model-data comparison for orbit 6 and part of orbit 7, overplotted with the crustal field (red dashed lines) and local time (gray dashed line only in Figure 2 (bottom)). It shows that in the strong crustal field regions (regions 1 and 3), the total magnetic field closely follows the crustal field with only small contributions from the induced field. In the weak crustal field region (regions 2 and 4), the induced field dominates and significantly improves the agreement. Also note that both regions 2 and 4 are in the dayside crossing, as indicated by the local time, so that the induced fields are relatively strong relative to the night side passage.

Generally, the good model-data agreement near the strong crustal field region indicates that the crustal field model [*Arkani-Hamed*, 2001] included in the MHD model is quite accurate. Around the dayside weak crustal field region, the induced field is needed to match the observations. The discrepancy between the data and model results could be caused by three different factors: (1) the variation in the solar wind (pressure and IMF direction change), (2) the inaccuracy in the crustal field model, and (3) the limitation of the MHD model that is used in the study.

Sometimes it is possible to identify the cause of the discrepancy. For example, the discrepancy around 10:10–10:20 UT for B_z is likely caused by the inaccuracy of the crustal field model, since the induced field normally could not cause such a big difference. However, in most cases, it is hard to distinguish the main source that contributes to the discrepancy, for example, the discrepancy in B_x around 10:20 UT. The overall good agreement between the model and observations indicates that the crustal field model is quite accurate and the single-fluid MHD model works well at MGS circular orbit (around 400 km altitude).

We also calculate the ion escape rates throughout the day as shown in Figure 3. The escaping plasma is dominated by O_2^+ for the majority of the day. The averaged total ion escape rate is about 2.3×10^{24} (s^{-1}), in the same range as the average heavy ion escape rate estimated from Mars Express (MEX) observations near solar minimum condition [*Lundin et al.*, 2013]. *Carlsson et al.* [2006] analyzed data from the Ion Mass Analyzer sensor on MEX to determine the mass composition of the escaping ion species at Mars, and they found that on average, the O_2^+/O^+ ratio is about 0.9, which is different from the mass composition that is predicted by

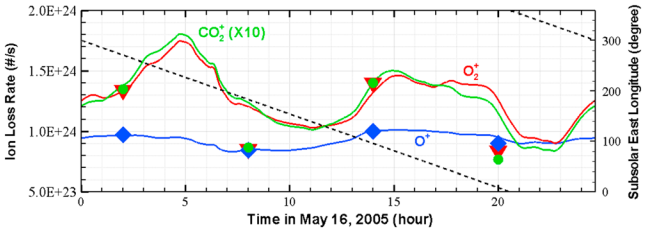

Figure 3. Variation of the modeled escape rates with time and subsolar east longitude. The solid lines are the integrated loss rates for O^+(blue), O_2^+(red), and CO_2^+(green, increased by a factor of 10 for better comparison) The black dashed line is the subsolar longitude. The symbols are the escape rates estimated using the steady state solution. Note that at 8 UT, the three symbols reside almost at the same location.

our simulation. However, their individual events show a wide spread of the ratio range from 0.2 to 2.0 (*Carlsson et al.* [2006], Figure 9), while the ratio of O_2^+/O^+ from our MHD model ranges from 0.9 to 1.8 for the specific day simulated. In addition, *Carlsson et al.*'s [2006] study was based on data collected from 23 April 2004 to 31 December 2004, which is in the declining phase (close to median solar activity). Our simulation results suggest that the dominant ion species (O^+ or O_2^+) largely depends on the solar cycle. For solar minimum condition, which is the case in our study, O_2^+ is the dominant species being lost to space, while for solar maximum condition, O^+ is the dominant one (see *Ma et al.* [2014]). Note that in the plot, the escape rate of CO_2^+ is enlarged by a factor of 10 for easy comparison. The loss rates of the two heavy ions O_2^+ and CO_2^+ share very similar trends and vary significantly as the crustal magnetic field rotates with the planet. The loss rate of O^+, the dominant ion species at high altitude, has a much smaller variation with time. Also in the plot, we add predictions of escape rates using steady state solutions at four different times. These times correspond to the strong crustal magnetic source being in the dawn (2 UT), subsolar (8 UT), dusk (14 UT), and midnight (20 UT) sectors, respectively. The escape rates are represented by symbols for comparison. As can be seen from the plot, the steady state solution can reproduce quite well only the escape rates of O^+. The escape rates for the heavy ions are significantly less from the time-dependent simulation results at 8 UT and 20 UT. The difference for O_2^+ is about 30% of the corresponding time-dependent results. This demonstrates that the ionosphere system needs time to respond to the continuous changes of the crustal field and that the interaction process cannot be simply assumed to be under a steady state. Thus, we should be cautious when using steady state solutions to approximate the escape rates, especially for the heavy ions. Also, the ion escape rates for the two heavy ions reach a local minimum near 11 UT, which is about 3 h after the strong crustal field passing by subsolar location, indicating in a general anticorrelation with the strength of the crustal field near subsolar region, consistent with what was found by *Ma and Nagy* [2007]. As suggested by *Lundin et al.* [2011], when the dayside strong crustal magnetic field anomalies interact with the solar wind, "minimagnetospheres" form and act as cellular structures, which effectively reduce the tailward transport and escape of ionospheric plasma. The escape rates peak when the strong crustal source is located in the morning and afternoon sectors and dip near noon and midnight. As mentioned in the Introduction, *Nilsson et al.* [2011] found that the escape rate is statistically significantly higher (by about 50%) from the northern quadrant than from the southern quadrant. We also examined the loss rates versus locations from our model results and found that when the crustal field is located near the morning and noon sectors, the escape rates from the northern quadrant is about twice the value from the southern quadrant. While when the crustal field is located near dusk and midnight, the escape rates from the two quadrants are about the same. The detailed relation between escape rates and crustal field location will be investigated in more detail in future studies.

Figure 4 shows the MGS latitude and solar zenith angle (SZA), simulated plasma density, plasma flow velocity, and magnetic field strength along a few orbits during the day. As shown in the figure, the dominant ion species is still O_2^+ even at 400 km altitude along MGS orbits. O^+ never exceeds O_2^+ during the whole period. The densities of the planetary ions show clear dependence on SZA as expected. Also during daytime passes, we usually see double peaks in the O_2^+ density. This is caused by the changes in ram angle (which is the same as SZA). The dips usually happen very close to the SZA minimum location when the crustal field is weak (for example, near 14 UT) or have a small time shift when the crustal field near the SZA minimum is strong. This is because when the crustal field is negligible, the ionosphere is more compressed at smaller SZA due to larger normal solar wind dynamic pressure. The peak of the O_2^+ density also has a clear correlation with the peak crustal magnetic field strength. When the crustal field is strongest near 12 UT, the peak density of O_2^+ is almost twice as large as the other peaks. The main reason for the density increase is the expansion of the ionosphere to high altitude with the help of the magnetic field pressure (mainly contributed by the crustal field) to

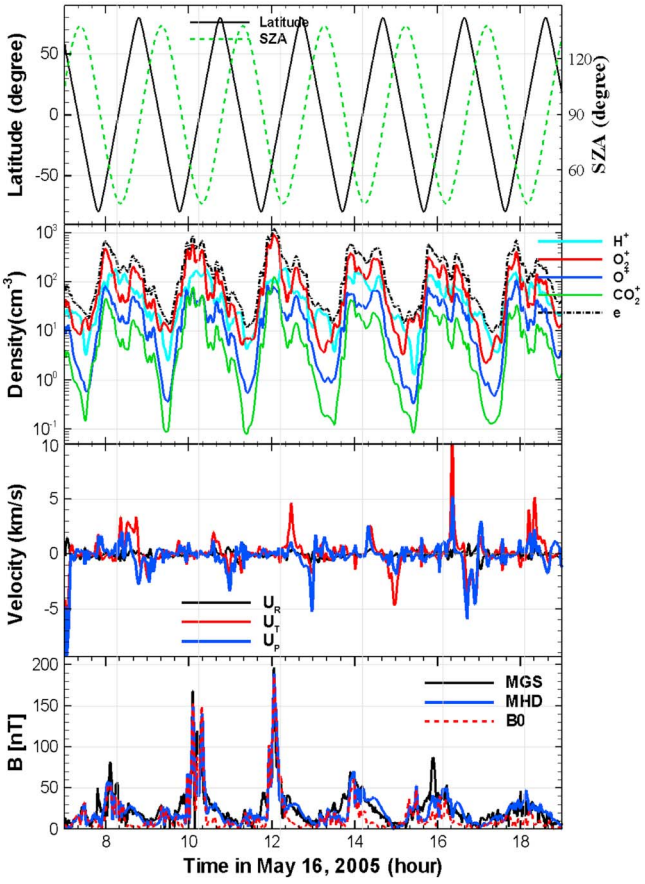

Figure 4. MGS latitude and local time, simulated plasma density, simulated plasma flow velocity, and simulated and observed magnetic field strength along several orbits. In Figure 4 (bottom), B_0 is the strength of the crustal field.

stand off the incoming solar wind plasma flow. The plasma flow was normally small in the radial direction along the MGS orbit as shown in the third panel, but can sometimes have a significant component in theta and phi directions. The large flow is normally predicted when MGS is above the equator shortly after the density minimum and was moving in a direction diverting around the planet: positive UT when MGS is in dayside, then negative when MGS moves into the nightside.

4. Summary

In this study we investigated how the rotation of Mars and its crustal magnetic field affect the solar wind interaction using a time-dependent multispecies MHD model. The model results closely agree with the MGS magnetometer observations along almost all of the 12 orbits we have simulated. It also found that the simulated ion loss rates slowly vary with the subsolar longitude, anticorrelating with the intensity of the dayside crustal field source, with some time delay. A steady state approximation can only reproduce reasonably well the escape rate of O^+, while the loss rates of heavy ions (O_2^+ and CO_2^+) are more time dependent. Model results also suggest that plasma distribution along the MGS orbit (around 400 km altitude) is significantly affected by the strong crustal field location, and O^+ density seldom exceeds O_2^+ density along the MGS orbit (400 km) during the whole period simulated. These findings could be tested using the observations of MEX and the upcoming NASA Mars Atmosphere and Volatile Evolution (MAVEN) mission.

This is the first time we have included the temporal variation of the rotating crustal magnetic field into a global interaction model of Mars. This is also a necessary step to have a meaningful comparison with spacecraft magnetometer observations and to predict what MAVEN will observe after it goes into orbit. The case presented here is for 16 May 2005, between southern spring and southern summer, for the solar minimum case (with subsolar latitude 13°S). This is similar to the season at the beginning of the mapping period of the MAVEN mission. We expect the variation of ion loss rates to be larger for southern summer, when the subsolar latitude is located farther in the southern hemisphere.

Acknowledgments

The work presented here was supported by the NASA grants NNX13A031G, NNG06GF31G and NNX11AN38G and the NSF grant AST-0908472. Resources supporting this work were provided by the NASA High-End Computing Program through the NASA Advanced Supercomputing Division at Ames Research Center. The MGS magnetic field observational data used in the study were obtained from the NASA Planetary Data System. The Space Weather Modeling Framework that contains the BATS-R-US code used in this study is publicly available from http://csem.engin.umich.edu/tools/swmf". For the distribution of the model results used in this study, please contact the corresponding author.

The Editor thanks two anonymous reviewers for their assistance in evaluating this paper.

References

Acuna, M. H., et al. (1998), Magnetic field and plasma observations at Mars: Initial results of the Mars Global Surveyor mission, *Science*, *279*, 1676–1680.

Acuna, M. H., et al. (1999), Global distribution of crustal magnetization discovered by the Mars global surveyor MAG/ER experiment, *Science*, *284*, 790–793.

Arkani-Hamed, J. (2001), A 50-degree spherical harmonic model of the magnetic field of Mars, *J. Geophys. Res.*, *106*, 23,197–23,208, doi:10.1029/2000JE001365.

Brain, D. A. (2006), Mars Global Surveyor measurements of the Martian solar wind interaction, *Space Sci. Rev.*, *126*(January), 77–112, doi:10.1007/s11214-006-9122-x.

Brain, D. A., J. S. Halekas, R. Lillis, D. L. Mitchell, R. P. Lin, and D. H. Crider (2005), Variability of the altitude of the Martian sheath, *Geophys. Res. Lett.*, *32*, L18203, doi:10.1029/2005GL023126.

Brain, D. A., et al. (2010), A comparison of global models for the solar wind interaction with Mars, *Icarus*, *206*(1), 139–151, doi:10.1016/j.icarus.2009.06.030.

Carlsson, E., et al. (2006), Mass composition of the escaping plasma at, *Icarus*, *182*, 320–328, doi:10.1016/j.icarus.2005.09.020.

Connerney, J. E. P., M. H. Acuña, P. J. Wasilewski, N. F. Ness, H. Rème, C. Mazelle, D. Vignes, R. P. Lin, D. L. Mitchell, and P. A. Cloutier (1999), Magnetic lineations in the ancient crust of Mars, *Science*, *284*, 794–798.

Crider, D. H., D. Vignes, A. M. Krymskii, T. K. Breus, N. F. Ness, D. L. Mitchell, J. A. Slavin, and M. H. Acuña (2003), A proxy for determining solar wind dynamic pressure at Mars using Mars Global Surveyor data, *J. Geophys. Res.*, *108*(A12), 1461, doi:10.1029/2003JA009875.

Fang, X., M. W. Liemohn, A. F. Nagy, J. Luhmann, and Y. Ma (2010), On the effect of the martian crustal magnetic field on atmospheric erosion, *Icarus*, *206*, 130–138, doi:10.1016/j.icarus.2009.01.012.

Kallio, E., J.-Y. Chaufray, R. Modolo, D. Snowden, and R. Winglee (2011), Modeling of Venus, Mars, and Titan, *Space Sci. Rev.*, *162*(1–4), 267–307, doi:10.1007/s11214-011-9814-8.

Ledvina, S. A., Y. J. Ma, and E. Kallio (2008), Modeling and simulating flowing plasmas and related phenomena, *Space Sci. Rev.*, doi:10.1007/s11214-008-9384-6.

Lundin, R., S. Barabash, M. Yamauchi, H. Nilsson, and D. Brain (2011), On the relation between plasma escape and the martian crustal magnetic field, *Geophys. Res. Lett.*, *38*, L02102, doi:10.1029/2010GL046019.

Lundin, R., S. Barabash, M. Holmström, H. Nilsson, Y. Futaana, R. Ramstad, M. Yamauchi, E. Dubinin, and M. Fraenz (2013), Solar cycle effects on the ion escape from Mars, *Geophys. Res. Lett.*, *40*, 6028–6032, doi:10.1002/2013GL058154.

Ma, Y. J., X. Fang, A. F. Nagy, C. T. Russell, and G. Toth (2014), Martian ionospheric responses to dynamic pressure enhancements in the solar wind, *J. Geophys. Res. Space Physics*, *119*, 1272–1286, doi:10.1002/2013JA019402.

Ma, Y., A. F. Nagy, I. V. Sokolov, and K. C. Hansen (2004), Three-dimensional, multispecies, high spatial resolution MHD studies of the solar wind interaction with Mars, *J. Geophys. Res.*, *109*, A07211, doi:10.1029/2003JA010367.

Ma, Y.-J., and A. F. Nagy (2007), Ion escape fluxes from Mars, *Geophys. Res. Lett.*, *34*, L08201, doi:10.1029/2006GL029208.

Modolo, R., G. M. Chanteur, and E. Dubinin (2012), Dynamic Martian magnetosphere: Transient twist induced by a rotation of the IMF, *Geophys. Res. Lett.*, *39*, L01106, doi:10.1029/2011GL049895.

Nagy, A., et al. (2004), The plasma environment of Mars, *Space Sci. Rev.*, *111*, 33–114.

Nilsson, H., et al. (2011), Heavy ion escape from Mars, influence from solar wind conditions and crustal magnetic fields, *Icarus*, *215*(2), 475–484, doi:10.1016/j.icarus.2011.08.003.

Powell, K. G., P. L. Roe, T. J. Linde, T. I. Gombosi, and D. L. DeZeeuw (1999), A solution-adaptive upwind scheme for ideal magnetohydrodynamics, *J. Comp. Phys.*, *154*, 284–309.

Toth, G., et al. (2012), Adaptive numerical algorithms in space weather modeling, *J. Comput. Phys.*, *231*(3), 870–903, doi:10.1016/j.jcp.2011.02.006.